July 17-22, San Francisco, California, USA

IPACK2005-73118

Thermal Optimal Design for Partially-Confined Compact Heat Sinks

M. P. Wang, H. T. Chen, J. T. Horng, T. Y. Wu, P. L. Chen and Y. H. Hung
Department of Power Mechanical Engineering
National Tsing Hua University
Hsinchu 30013, Taiwan
e-mail: yhhung@pme.nthu.edu.tw

ABSTRACT

An effective method for predicting the optimal thermal performance of partially-confined compact heat sinks under multi-constraints of pressure drop and heat sink mass has been successfully developed. The design variables of PPF compact heat sinks include: heat sink fin and base material, thickness of heat sink base, heat flux, channel top bypass and inlet flow velocity. A total of 108 experimental cases for confined forced convection are designed by the Central Composite Design (CCD) method. According to the results in ANOVA, a sensitivity analysis for the design factors is performed. From the analysis, the effect of inlet flow velocity, which has the contribution percentage of 86.24%, dominates the thermal performance. The accuracies of the quadratic RSM models for both thermal resistance and pressure drop have been verified by comparing the predicted response values to the actual experimental data. The maximum deviations of thermal resistance and pressure drop are 9.41% and 7.20% respectively. The Response Surface Methodology is applied to establish analytical models of the thermal resistance and pressure drop constraints in terms of the key design factors with a CCD experimental design. By employing the Sequential Quadratic Programming technique, a series of constrained optimal designs can be efficiently performed. The numerical optimization results for four cases under different constraints are obtained, and the comparisons between these predicted optimal designs and those measured by the experimental data are made with a satisfactory agreement.

INTRODUCTION

In recent years, heat sink is the most common thermal management device in the electronics industry due to its simple configuration and cheap cost. In cooling electronic packages, a heat sink is a very effective heat removal device to provide an additional surface for convection under the condition of natural convection flow and forced convection flow.

The heat sink can be defined as a heat dissipater that operates as a result of the temperature difference and thermal resistances between the electronic package and the ambient air. The functions of using heat sinks are (1) to improve the thermal control of electronic components, assemblies, and modules by enhancing their exterior surface area through the use of fins or spines; and (2) to enhance both the reliability and functional performance of electronics, telecommunication, and power conversion systems. Simplicity and cost effectiveness are the advantage of using air-cooled heat sinks.

The parallel-plate fin (PPF) heat sinks are often used to improve cooling performance of electronic components, assemblies, and modules by enhancing their heat-dissipating surface area through the use of fins. Due to the necessary of cooling design, many investigators had given effort in studying forced convection of the parallel-plate fin heat sinks.

Generally, the compactness of a heat sink can be defined as the ratio of the overall heat-dissipating surface area to the volume of heat sink. The ratio is between 1.2 and 3.6 m^2/m^3 for commercial heat sinks. In the present study, the ratio of the so-called "compact" heat sinks employed is 8.3 m^2/m^3.

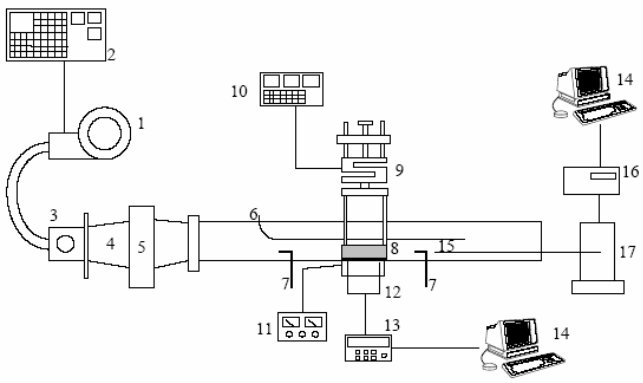

Fig.1 Overall Experimental Setup with Relevant Measuring

System for Forced Convection Channel Flow

In most practical cases, heat sinks operate with clearance space around them. Such clearance allows part of the cooling flow to bypass the core of the heat sinks. The hydraulic and thermal performances of heat sinks are heavily influenced by the bypass effect; and there are two factors must be considered for the designers: (1) The performance of the heat sink is also a function of the size of the wind tunnel relative to the size of the heat sink; and (2) The airflow resistance of the heat sink is important for understanding how much pumping power is needed.

Furthermore, the design of heat sinks requires difficult trade-offs between conflicting parameters, e.g. mass, maximum pressure drop and space constraints; and these parameters influence one another. These constraints add to the complexity and challenges of the thermal design. Thus, the optimal thermal design of compact heat sinks is becoming one of the primary challenges of packaging tasks.

THE EXPERIMENTS

Figure 1 shows the overall experimental setup with the relevant apparatus and instruments for forced convection channel flow. The present experimental facilities are composed of five major parts: (1) air supply facilities, (2) pressure load unit, (3) test section, (4) TSI unit, (5) apparatus and instrumentation.

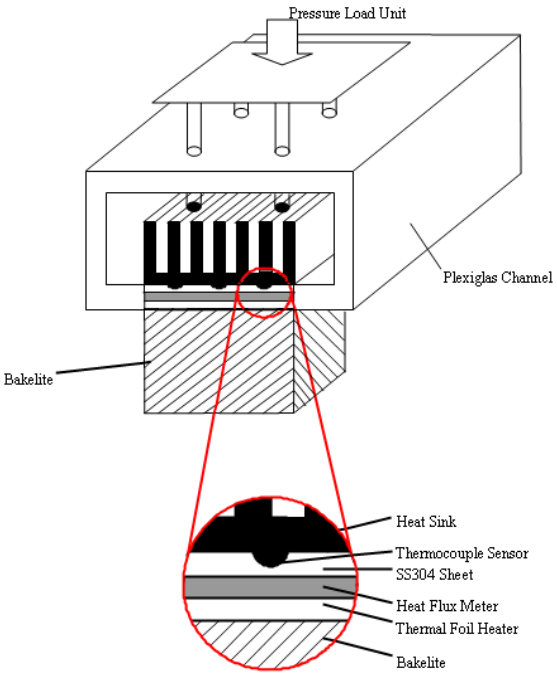

Fig. 2 Schematic of Test Section

Test Section

Figure 2 shows the test section and test assembly, respectively. The width of the test section is 82 mm and with flexible channel height. The heat sink test assembly is properly sealed and installed on the test plate. As shown in Fig.2, the test plate is composed of five components such as thermocouples, interface heat spreader (IHS), heat flux meter, thermal foil heater and insulated Bakelite block. To eliminate the need to groove each heat sink for testing multiple heat sinks, an interface heat spreader made of 0.8 mm thick stainless steel sheet (SS304) with a size of 7.0x7.0cm^2 is installed on the top of test plate. Nine grooves (0.8mm wide and 0.4mm deep) are milled on one side of the interface heat spreader, and nine calibrated 40-guage T-type thermocouples placed in the grooves using thermally-conductive epoxy. The testing compact heat sink is placed on the top of the heat spreader. Figure 3 shows the photo of a typical compact heat sink. In order to accurately measure the heat flux flowing to the heat sink, a precise heat flux meter (Omega, Model HFS-3) is used in the experiments. The heating load is generated by a 60 x 60 mm thermofoil heater having a thickness of 0.3 mm, which is centrally epoxied under the heat flux meter. The thermofoil heater has an electric resistance of 383.6 ohms and can generate heat on the heat sink with a voltage varied between 0 and 240 volts by series connecting two D.C. power supply (model: GW GPC-6030D, maximum operating ranges: 120V/3A). For maintaining same heat transfer conditions from heater to the heat sink base, the material of Kapton, which is the dame material of heat flux meter, is employed to makeup the vacant gaps between the locations without installing heat flux meter on the thermofoil heater and the stainless steel plate. The advantage of using heat flux meter is to avoid the complicated data reduction with an approximate evaluation of heat lossed in the traditional experiments.

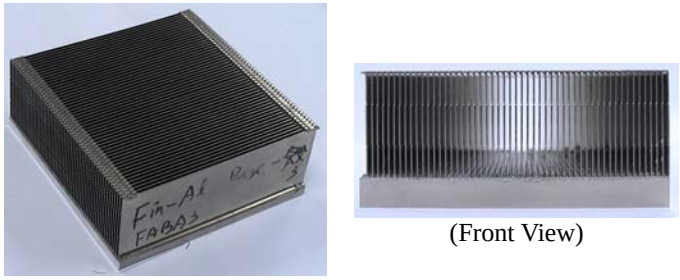

Fig.3 Photo of Compact Heat Sink

Data Reduction

For exploring heat transfer characteristics for confined heat sinks, a further data reduction is needed to transfer original measured data into heat transfer information. The objective of the data reduction in the experiments is to get the local and average heat transfer coefficients for heat sinks. The temperature can be measured from the data logger system; and the heat dissipation rate can be directly measured by the heat flux meter flush-mounted on the bottom surface of the heat sink. Thus, the local thermal resistance can be evaluated as

$$R_{th,x} = \frac{\Delta T_x}{Q} \qquad (1)$$

where ΔT_x is the difference between local temperature of heat

sink base at location x and air temperature at channel inlet, Q is the heat dissipation rate measured by the heat flux meter.

The total heat flux measured by the heat flux meter, q_t, is converted into the following three heat transfer modes at any specific transient time: (1) radiactive heat loss, q_r; (2) internal energy change in the heat sink, q_i; and (3) convective heat dissipated, q_C. That is,

$$q_c = q_t - q_r - q_i \tag{2}$$

This energy-balance equation calculates the net convective heat q_c dissipated from the heat sink to the air. q_r is the radiative heat loss from the heat sink surface to its surroundings. According to the results of radiation analysis, the maximum radiative heat losses are less than 0.59% of the total heat flux for forced convection in the present study. The q_i is the internal-energy change of the heat sink during the experimental period.

Before the experimental results of the transient and steady-state condition are displayed, it is necessary to clarify the steady state of each experiment. Usually, the steady-state condition is considered to be achieved when q_i approaches zero; and the q_C variation with time is less than 1.0% of the previous q_C value in each experiment. Accordingly, the power-on transient period is defined as the time elapsed to achieve the steady-state condition after the power switched on.

The transient local and stagnation Nusselt numbers can be respectively defined as

$$Nu_x = \frac{h_x L_H}{k_a} = \frac{q_{c,x} L_H}{(T_{B,x} - T_a)k_a} \tag{3}$$

where L_H is the entire length of heat sink base. $T_{B,\,x}$ and T_a represent the local base temperature and air temperature at channel inlet, respectively. $q_{c,\,x}$ is the transient local convective heat flux.

The average heat transfer coefficient of the heat sinks in the study can then be evaluated with the following equation

$$\bar{h} = \frac{\bar{q}_c}{(\bar{T}_B - T_a)} \tag{4}$$

Accordingly, the transient average Nusselt number based on the length of heat sink can be defined as $\overline{Nu} = \frac{\bar{h} L_H}{k_a}$.

Test Matrix

For exploring the forced convection heat transfer characteristics for compact PPF heat sinks, the influencing parameters and conditions studied are listed in Table 1. As shown in Fig.4, they include the fin material, base material, base thickness, heat flux, top bypass and inlet flow velocity. There are a total of 108 cases with various parameter combinations in the present experiments.

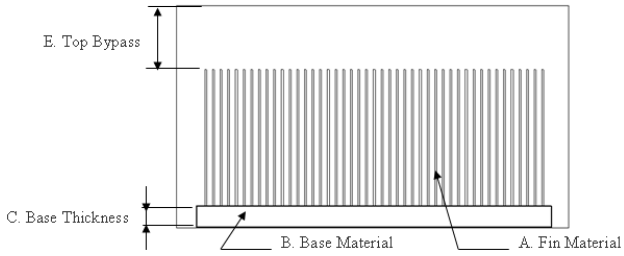

Fig.4 Parameters Explored in the Study

Table 1 Range of Experimental Parameters for Compact PPF Heat Sinks in Forced Convection

Fin Material	Al, Cu				
Base Material	Al, Cu				
Channel Width W_C (mm)	82.0				
Side Bypass (W_C-W)/2 (mm) (W_C-W)/2W_C	9.3 0.11				
Top Bypass (mm) H/H_C	0 1	8.4 0.82	16.9 0.64	25.3 0.56	33.7 0.47
Base Thickness H_B (mm)	3	6	9	12	15
Heat Flux(W/m^2) Gr_S	2607.3 1.7×10^5	5866.4 2.8×10^5	9125.5 5.1×10^5	12384.6 8.4×10^5	15643.7 1.0×10^6
Inlet Flow Velocity U_i (m/s) Re_D	2.0 7823	3.5 14232	5.0 19076	6.5 26428	8.0 30767

Uncertainty Analysis

Uncertainty and sensitivity analysis is extensively used in the experimental planning stage to help design the apparatus and data reduction procedures. After the main experiment is in place an n'th order uncertainty analysis will be performed to determine the uncertainty range in the main measured quantities, e.g., heat transfer coefficient, Nusselt number, etc.. The method is using the standard single-sample uncertainty analysis recommended by Moffat [1].

According to the uncertainty analysis, the results of uncertainty analysis for confined heat sinks reveal that the average uncertainties of air flow velocity, Reynolds number and average heat transfer coefficient in the steady-state period are 1.97%, 2.23% and 9.73%, respectively.

THERMAL OPTIMAL DESIGN

As we know, the motivation for optimal design is to obtain the optimal thermal performance with the practical constraints such as available pressure drop, volume, and mass/weight trade-offs. However, it becomes very difficult for designers to foresee all the consequences of changing certain design variables in such a multidisciplinary problem due to the complex interactive relationship among the design variables and responses. Consequently, the complicated task may only be solved with the design optimization technique. With the

methodology of thermal optimal design presented by Chen et al. [2], the thermal optimal design for partially-confined compact heat sinks has been systematically performed in the following.

Design Variables of Compact Heat Sinks

The design variables of PPF compact heat sinks include: heat sink fin and base material, thickness of heat sink base, heat flux, channel top bypass and inlet flow velocity. The five levels for each design variables for practical compact heat sinks design for confined forced convection are listed in Table 2.

Table 2 Practical Ranges of Design Variables for Partially-Confined Compact Heat Sinks in Forced Convection

Design Variables	Coded Value of the Design Variables				
	Lowest	Low	Center	High	Highest
A: Fin Material		Al		Cu	
B: Base Material		Al		Cu	
C: Base Thickness(mm)	3	6	9	12	15
D: Heat Flux(W/m^2)	2607.3	5866.4	9125.5	12384.6	15643.7
E: Top Bypass(mm)	0.0	8.4	16.9	25.3	33.7
F: Inlet Flow Velocity(m/s)	2.0	3.5	5.0	6.5	8.0

Design of Experiments

In conventional one-factor-at-a-time experimentation, the experimenter varies a single factor while all other factors are held as constants, thereby ignoring the effect of interaction among the factors. The design of experiments (DOE) is a systematic statistical approach to explore the relationships between design variables and responses that can give a better overall system understanding. In addition, all of this is accomplished with the minimal number of experiment runs. Well-chosen experimental designs maximize the amount of information that can be obtained for a given amount of experimental effort.

Response Surface Methodology

The major problem concerned in multidisciplinary design optimization is how to obtain the necessary information to guide toward the optimal solution within a reasonable time. Furthermore, since the performance analysis for heat sinks are rather complex and include iterative solution procedures, only an implicit relationship between objective functions and design variables can be found theoretically. The optimization DOE technique applied in this study, therefore, can construct the statistical formulation (explicit form) of the design problem, including the design objectives and constraints.

Response Surface Methodology (RSM) is an effective tool for establishing the explicit relationship of an unknown system. RSM procedures seek to find the relationship between design variable and response and determine the optimum system response through statistical fitting method using observed datum. Moreover, the RSM offers a systematic and efficient approach because the effects of design variables can be decoupled with the help of ANOVA, and the obtained response surface model can provide the designer with an overall perspective of the system response according to the behavior of design variables within a design space.

The response surface methodology is well adapted to make an analytical model for the complicated problem. RSM provides an approximate relationship between a true response η and k design variables, which is based on the observed data from the process or system.

The response is generally obtained from real experiments or computer simulations, and the true response η is the expected response. We suppose that the true response η can be written as

$$\eta = F(x_1, x_2, ..., x_k) \tag{5}$$

where $x_1, x_2, ..., x_k$ in Eq.(5) are the design variables. The experimentally obtained response y differs from the expected value η due to random experimental error. Because the form of the true response function F is unknown and perhaps very complicated, we must approximate it. The relation between y and η may be written as

$$y = F(x_1, x_2, ..., x_k) + \varepsilon \tag{6}$$

where ε denotes the random error, which includes measurement error on the response and is inherent in the process or system. We treat ε as a statistical error, often assuming it to have a normal distribution with mean zero and variance σ^2. In many cases, the approximating function F of the true response η is normally chosen to be either a first-order or a second-order polynomial model, which is based on Taylor series expansion.

For the better accuracy, the second-order model is used in this paper. The general form for the second-order model is expressed as

$$y = \beta_0 + \sum_i \beta_i x_i + \sum_i \beta_{ii} x_i^2 + \sum_{i<j} \beta_{ij} x_i x_j + \varepsilon \tag{7}$$

where β_i represents the linear effect of x_i, β_{ii} represents the quadratic effect of x_i, β_{ij} represents the linear-by-linear interaction between x_i and x_j, and ε is the fitting error.

An analysis of a second-order experiment can be done by approximating the response surface relationships with a fitted second-order regression model. The regression coefficients of the predictive model are estimated by the method of least squares according to Myers and Montgomery [3].

Central Composite Design

An experimental design for fitting a second-order model

must have at least three levels of each factor, therefore, the 3^k Factorial Design is required. However, it is rarely used in practice for large k (the number of design variables) because the number of experimental runs is too large. The Central Composite Design (CCD) is the most widely used method and is applied in this paper for better efficiency. The CCD consists of a 2^k factorial or 2^{k-p} fractional factorial design, augmented by additional axial points and center points. This design provides five levels for each design variable, and the total number of experiment runs N is calculated by

$$N = 2^k + 2k + n_0 \tag{8}$$

where 2^k represent factorial points, $2k$ represent the axial points, and n_o are center points.

The design points are represented graphically in Fig.5. With the observed data from the CCD experiments, the regression coefficients of the predictive model can be estimated by the method of least-square. The resulting response surface quadratic model equations can be obtained.

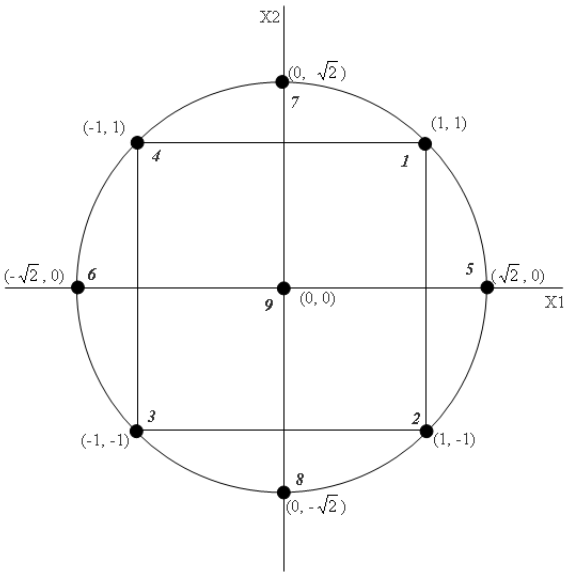

Fig. 5 Central Composite Design for Two-Factor Experiments

A total of 108 experimental cases for confined forced convection are designed by the CCD method in this study. The analysis of variance for thermal resistance of confined forced convection is conducted. Diagnostic analysis of the residuals from the above regression model may reveal errors that were not in Gaussian distribution, which is one of the important assumptions of experimental analysis; Box-Cox power transformation is a useful method to make the response variance close to the normal distribution [4]. In the case of forced convection, an *Inverse* transformation is applied.

With the observed data from the CCD experiments, the regression coefficients of the predictive model can be estimated by the method of least-squares.

Sensitivity Analysis

According to the results in ANOVA, a sensitivity analysis for the design factors is performed and shown in Fig.6. With this systematic statistical method, instead of one-factor-at-a-time experimentations, a quicker and better overall system understanding can be obtained. From the results, the effect of inlet flow velocity (F, 86.24%) dominates the thermal performance. For more intuitional information, the one-factor variation plot can also be examined in seconds form the established response surface model; however, for a complex system, only considering the one-factor variation plot might lead to a misinterpretation because of the interactive effects across factors.

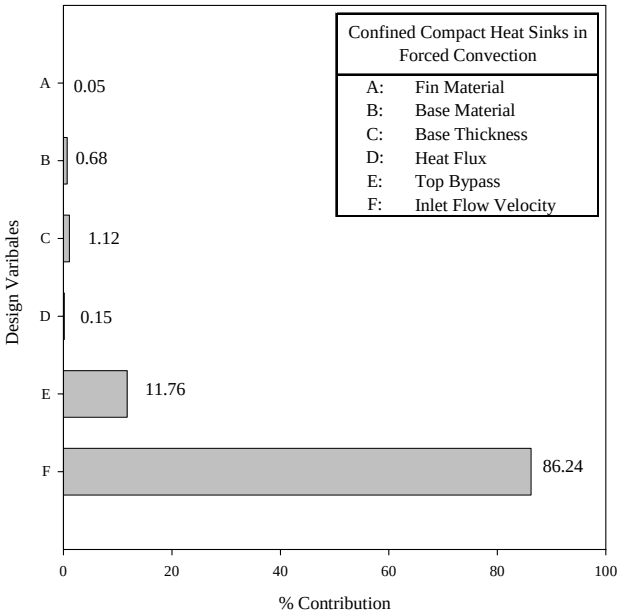

Fig. 6 Sensitivity Analysis of Design Variables for Confined Compact Heat Sinks in Forced Convection

Model Accuracy Evaluation

The accuracy of the quadratic RSM models is evaluated by comparing the predicted response values to the actual experimental data. As shown in Figs.7 and 8, good fitting accuracies are obtained. The maximum and average deviations of thermal resistance for partially-confined compact heat sinks in forced convection are 9.41% and 2.21%, respectively. The maximum and average deviations of pressure drop for confined compact heat sink in forced convection are 7.20%, and 1.11%, respectively. Since the explicitly expressed quadratic model is close enough to the actual system, the optimal design can be found by applying the numerical optimization algorithms.

Numerical Optimization

The constrained optimization problem is solved by the Sequential Quadratic Programming (SQP) method in this thesis. SQP methods can be interpreted as Newton's method applied to the solution of the Karush-Kuhn-Tucker (KKT) conditions [5].

The objection is augmented using Lagrange multipliers and an exterior penalty so that the resulting one-dimensional search is unconstrained.

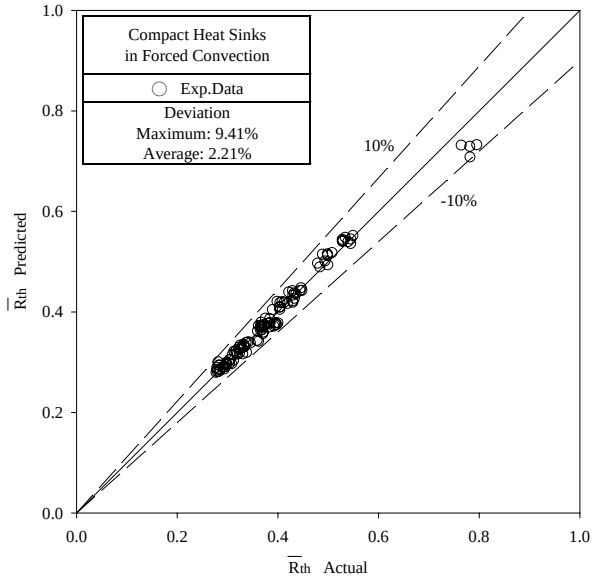

Fig.7 Modeling Accuracy Plot for Thermal Resistance of Confined Compact Heat Sinks in Forced Convection

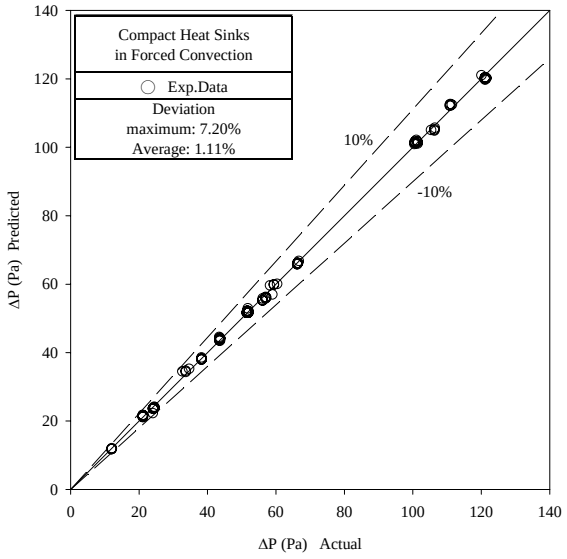

Fig.8 Modeling Accuracy Plot for Pressure Drop of Confined Compact Heat Sinks in Forced Convection

At first, an optimization problem is defined as follows:

Case(I)

Minimize: $Rth(\boldsymbol{X})$ $\boldsymbol{X} = \{A, B, C, D, E, F\}$

Subject to: $\boldsymbol{X}_L \leqq \boldsymbol{X} \leqq \boldsymbol{X}_U$

where $\boldsymbol{X}_L$ *and* $\boldsymbol{X}_U$ are the lower and upper boundaries of the design variable respectively.

That is, to minimize the thermal resistance $Rth(\boldsymbol{X})$ with only the boundary limits of design variables $\boldsymbol{X}$. The optimization results for Case(I) can be easily comprehended and are listed in Table 3. All the design variables are moving to the boundary limits that will decrease the thermal resistance. However, this design will result in the impractical large pressure drop of 256.26 Pa and heavy weight of 703.3 g. In spite of the excellent thermal resistance, this design needs a further improvement with more practicality in consideration.

When the pressure drop constraint is taken into consideration, the task of the optimization becomes to minimize the thermal resistance with the constraint of pressure drop be less than 120 Pa for practical use and the design variables be in the acceptable ranges. The optimization problem formation is then expressed as follows:

Case(II)

Minimize: $Rth(\boldsymbol{X})$ $\boldsymbol{X} = \{A, B, C, D, E, F\}$

Subject to: $\Delta P(\boldsymbol{X}) \leqq 120\ Pa$

$\boldsymbol{X}_L \leqq \boldsymbol{X} \leqq \boldsymbol{X}_U$

where $\boldsymbol{X}$ are the design variables; $Rth(\boldsymbol{X})$ is the objective function, thermal resistance; $\triangle P(\boldsymbol{X})$ is the constrain function, pressure drop; and $\boldsymbol{X}_L$ *and* $\boldsymbol{X}_U$ are the lower and upper boundaries of the design variable respectively.

The optimization results for Case(II) are listed in Table 3. As compared with the optimal design with only boundary limits, it can be found that the thermal resistance for the case with ΔP constraint slightly increased to 0.258, but the pressure drop was down to the suitable 119.99 Pa instead of the impractical 256.26 Pa.

Then, when the mass constraint, instead of pressure drop constraint, is taken into consideration, the task of the optimization becomes to minimize the thermal resistance with the constraint of mass be less than 400 g for practical use and the design variables be in the acceptable ranges. The optimization problem formation is then expressed as follows:

Case(III)

Minimize: $Rth(\boldsymbol{X})$ $\boldsymbol{X} = \{A, B, C, D, E, F\}$

Subject to: $Mass(\boldsymbol{X}) \leqq 400\ g$

$\boldsymbol{X}_L \leqq \boldsymbol{X} \leqq \boldsymbol{X}_U$

The optimization results for Case(III) are listed in Table 3. As compared with the optimal design with only boundary limits, it can be found that the thermal resistance for the case with mass constraint increased to 0.238, but the mass was down to the suitable 399.9 g instead of the overweight 703.3 g. However, the pressure drop of this drop becomes even larger. Therefore, these constraints must be considered simultaneously so that the optimal design can satisfy all the design requirements without time-consuming trial-and-error iteration designs.

When the pressure drop constraint and mass constraint are taken into considerations, the task of optimization becomes to minimize the thermal resistance with the constraint of pressure drop be less than 120 Pa, mass be less than 400 g, and the design variables be in the acceptable ranges. The optimization problem formation is then expressed as follows:

Case(IV)

Minimize: $Rth(\boldsymbol{X})$ $\boldsymbol{X} = \{ A, B, C, D, E, F \}$

Subject to: $\Delta P(\boldsymbol{X}) \leqq 120\ Pa$

$Mass(\boldsymbol{X}) \leqq 400\ g$

$\boldsymbol{X}_L \leqq \boldsymbol{X} \leqq \boldsymbol{X}_U$

The optimization results for Case(IV) are listed in Table 3. All the pressure drop and mass constraints were satisfied the design goals, and the thermal resistance is minimized at the same time. As compared with the optimal design with only boundary limits, it can be found that the thermal resistance for the case with pressure drop and mass constraint increased to 0.259, but the mass was down to the suitable 165.9 g, pressure drop pressure drop was down to the suitable 119.99 Pa. Therefore, with the developed optimizer to efficiently seek the optimal heat sink, the product-developing cycle or the time-to-market can be significantly shortened. In addition, all the predicted optimal results based on the response surface models, as shown in Table 3, were compared with the theoretical calculations; and a good agreement was made with maximum deviation less than 8.03%.

Table 3 Optimization Results

	A Fin Material	B Base Material	C Base Thickness	D Heat Flux	E Top Bypass	F Ui	Rth	△P	Mass
Case(I)	Optimal Design with Boundary Limits Only								
Prediction	Cu	Cu	15.0	60.0	0.0	8.0	0.236	256.26	703.3
Experiment	Cu	Cu	15.0	60.1	0.0	8.0	0.251	260.33	704.0
Deviation%							6.26%	1.56%	0.10%
Case(II)	Optimal Design with Boundary Limits and △P ≦120Pa Constraint								
Prediction	Cu	Cu	3.0	60.0	10.08	8.0	0.258	119.99	297.0
Experiment	Cu	Cu	3.0	59.7	10.0	8.0	0.279	121.39	300.0
Deviation%							7.46%	1.15%	1.01%
Case(III)	Optimal Design with Boundary Limits and Mass ≦400g Constraint								
Prediction	Al	Cu	9.8	60.0	0.0	8.0	0.238	224.19	399.9
Experiment	Al	Cu	9.0	59.7	0.0	8.0	0.259	227.32	371.0
Deviation%							8.03%	1.38%	7.79%
Case(IV)	Optimal Design with Boundary Limits, △P ≦120Pa and Mass ≦400g Constraint								
Prediction	Al	Cu	3.0	60.0	10.13	8.0	0.259	119.99	165.9
Experiment	Al	Cu	3.0	59.8	10.1	8.0	0.281	121.37	165.5
Deviation%							7.81%	1.14%	0.24%

To further demonstrate the capability of the developed optimizer, the optimization phenomenon can be further explored after the optimal design was found. For Case(I), from the viewpoint of the thermal performance, both C and E will be moved to the lower-right corner for the smallest thermal resistance (0.236 ^{o}C/W) as shown in Fig.9. For Case(II), with pressure drop added into design consideration, C and E need to move toward the left side for an acceptable design, as shown in Fig.10. It can be seen that the optimizer automatically find the minimal R_{th} (0.258 ^{o}C/W) under given maximum acceptable ΔP (120Pa). For Case(III), with mass constraint added into design consideration, C and E moved to the lower-center as shown in Fig.11. This is because some other factors had less effects (from the sensitivity analysis) on thermal resistance, were optimized for the smaller thermal resistance (0.238 ^{o}C/W) under given mass constraint (400 g). For Case(IV), with the pressure drop and mass constraints taken into considerations simultaneously, C and E were optimized as shown in Fig.12; and a not only acceptable but optimal design for all the design objectives and compromises was automatically obtained without the laborious trial-and-error procedure.

CONCLUDING REMARKS

A series of experimental investigations with stringent measurement methods on the studies related to the fluid flow and heat transfer for partially-confined compact heat sinks in forced convection have been successfully conducted. An effective method for predicting the optimal thermal performance of confined compact heat sinks under multi-constraints of pressure drop and heat sink mass has been successfully developed. Based on the results and discussion, the main conclusions emerged from this study are listed below:

(1) According to the results in ANOVA, a sensitivity analysis for the design factors is performed. From the results, the effect of inlet flow velocity (F, 86.24%) dominates the thermal performance.

(2) The accuracies of the quadratic RSM models for both thermal resistance and pressure drop have been verified by comparing the predicted response values to the actual experimental data. The maximum deviations of thermal resistance and pressure drop are 9.41% and 7.20% respectively.

(3) The Response Surface Methodology is applied to establish analytical models of the thermal resistance and pressure drop constraints in terms of the key design factors with a CCD experimental design. By employing the Sequential Quadratic Programming technique, a series of constrained optimal designs can be efficiently performed.

(4) The numerical optimization results for four cases under different constraints are obtained, and the comparisons between these predicted optimal designs and those measured by the experimental data are made with a satisfactory agreement.

ACKNOWLEDGEMENTS

The authors wish to thank the National Science Council, Taiwan, ROC for the support under the grant numbers NSC93-2212-E-007-002 and NSC93-2622-E-007-016-CC3.

REFERENCES

[1] Moffat, R. J., 1988, "Describing the Uncertainties in Experimental Results," *Expl. Thermal Fluid Sci.*, Vol.1, pp.3-17.

[2] Chen, H. T., Horng, J. T., Chen, P. L., and Hung, Y. H., 2004, "Optimal Design for PPF Heat Sinks in Electronics Cooling Applications," *ASME J. Electron. Packag.*, Vol. 126, pp.410-422.

[3] Myers, G. N., and Montgomery, D. C., 2002, *Response Surface Methodology*, 2nd Edition, John Wiley & Sons, New York.
[4] Box, G. E. P., and Draper, N. R., 1987, "Empirical Model-Building and Response Surfaces," John Wiley & Sons, New York.
[5] Vanderplaats, G. N., 1993, *Numerical Optimization Techniques for Engineering Design*, McGraw-Hill, Inc., New York.

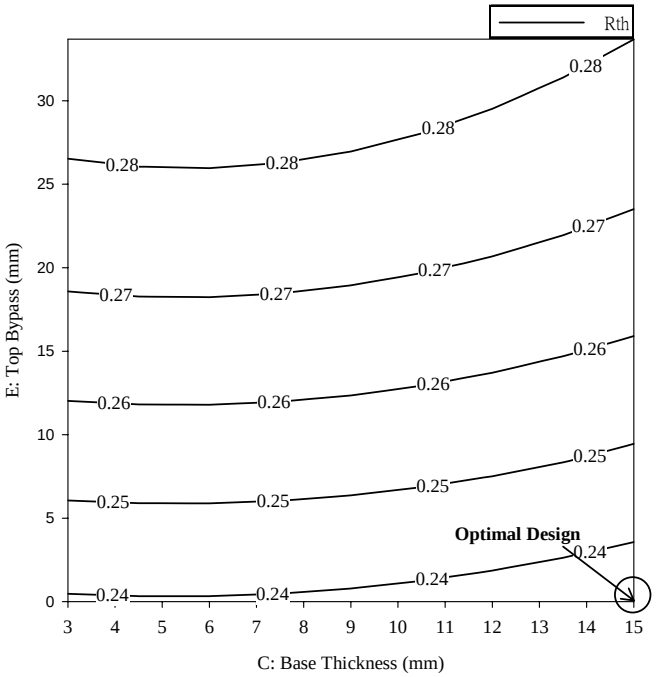

Fig.9 Case (I) Optimal Design Values of Base Thickness and Top Bypass with Boundary Limits Only

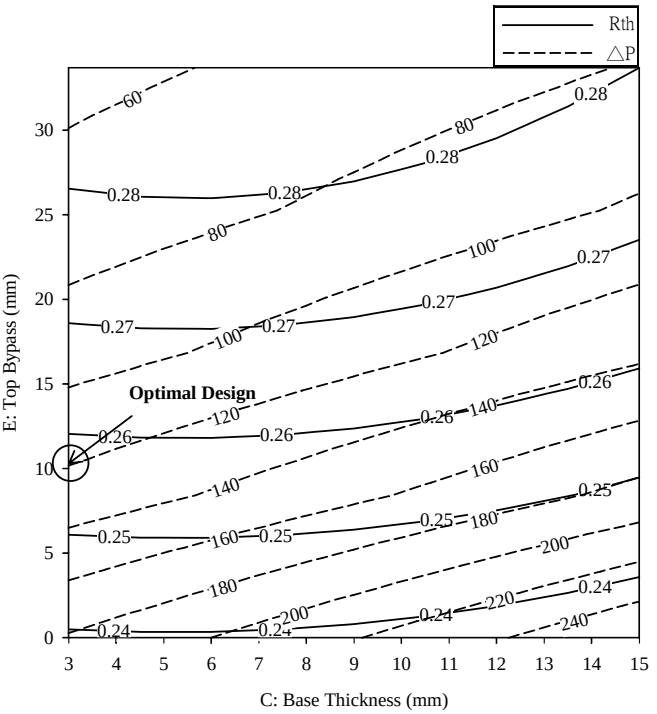

Fig.10 Case (II) Optimal Design Values of Base Thickness and Top Bypass with Boundary Limits and △P≦120 Pa Constraint

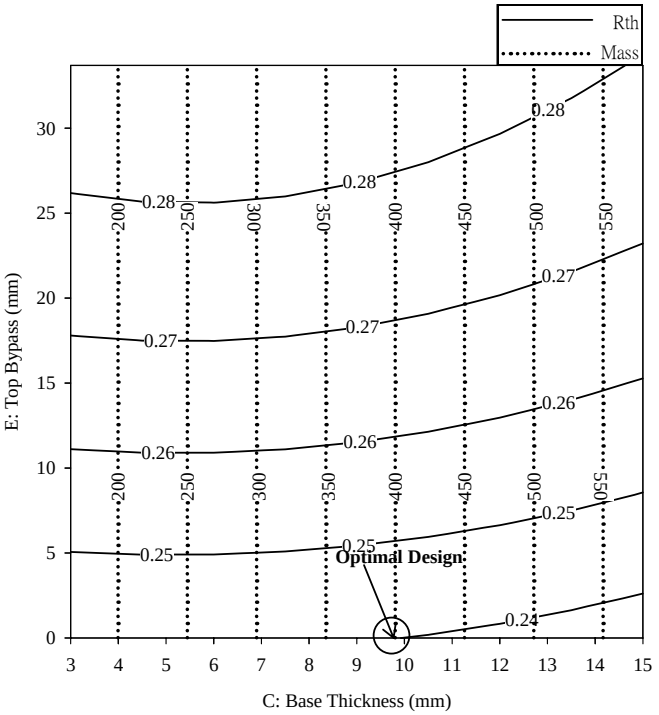

Fig.11 Case (III) Optimal Design Values of Base Thickness and Top Bypass with Boundary Limits and Mass≦ 400g Constraint

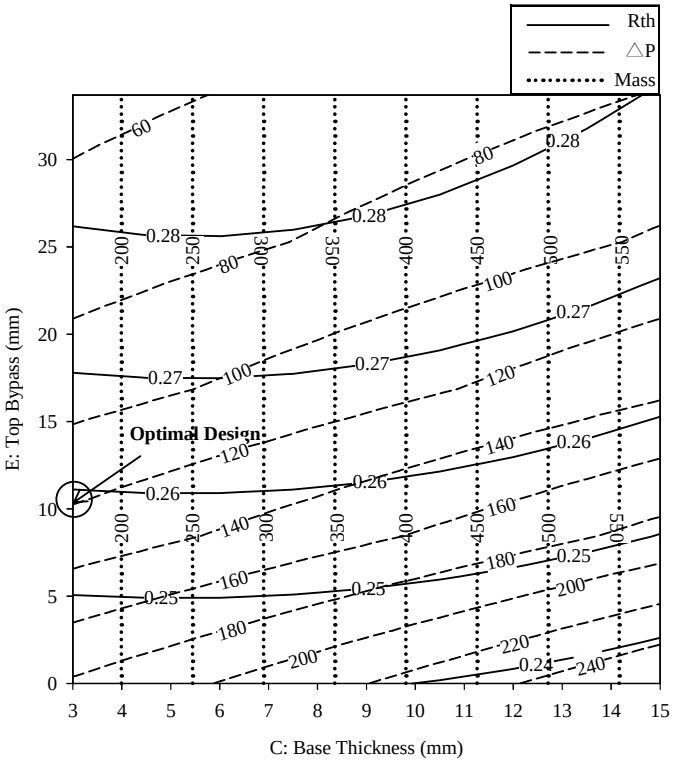

Fig.12 Case (IV) Optimal Design Values of Base Thickness and Top Bypass with Boundary Limits, △P≦120 Pa, and Mass≦ 400g Constraints